Structural Origins of the Enhancement in Ionic Conductivity of a Chalcogenide Compound by Adding AgI

Qiao, Wanchun; Qiao, Ang; Tao, Yunhang; Gu, Shaoxun; Yue, Yuanzheng; Tao, Haizheng

Published in:
ChemElectroChem

DOI (link to publication from Publisher):
10.1002/celc.201902163

Publication date:
2020

Document Version
Accepted author manuscript, peer reviewed version

FUNDAMENTALS & APPLICATIONS

CHEMELECTROCHEM

ANALYSIS & CATALYSIS, BIO & NANO, ENERGY & MORE

Accepted Article

Title: Structural origins of the enhancement in ionic conductivity of a chalcogenide compound by adding AgI

Authors: Wanchun Qiao, Ang Qiao, Yunhang Tao, Shaoxuan Gu, Yuanzheng Yue, and Haizheng Tao

To be cited as: *ChemElectroChem* 10.1002/celc.201902163

Link to VoR: http://dx.doi.org/10.1002/celc.201902163

A Journal of

ChemPubSoc Europe

WILEY-VCH

www.chemelectrochem.org

ARTICLE WILEY-VCH

Structural origins of the enhancement in ionic conductivity of a chalcogenide compound by adding AgI

Wanchun Qiao, [a] Ang Qiao,[a] Yunhang Tao, [b] Shaoxuan Gu, [a] Yuanzheng Yue, [a,c] Haizheng Tao * [a]

Abstract: Through a chemo-mechanical milling process, we prepare a highly conductive (1.1×10^{-3} S·cm^{-1}) amorphous $0.5AgI\cdot0.5Ag_3PS_4$ conductor. Detailed structural characterizations indicate that the significantly higher ionic conductivity in the amorphous $0.5AgI\cdot0.5Ag_3PS_4$ compared to Ag_3PS_4 can be ascribed to the formation of mixed polymeric anions $\{[PS4]_mI_n\}$ around Ag^+ ions. Through heat-treatment at 370 °C for 20 minutes, the room temperature ionic conductivity of the $0.5AgI\cdot0.5Ag_3PS_4$ conductor is further enhanced by about 4 times. This enhancement can be ascribed to the following two aspects: 1) the existence of residual amorphous phase with higher ionic conductivity; 2) the connection of the fast ionic conductive interfaces between the precipated Ag_7PS_6 nano-crystals and the residual amorphous phase. This work reveals the key roles of both disorder and interface in improving the ionic conductivity of solid state electrolytes.

Introduction

Compared to the liquid electrolytes currently used in commercial batteries, solid electrolytes have obtained extensive attention mainly owing to their highly applicable perspectives in stability (non-volatility),[1-4] safety (non-explosiveness)[5-9] and device fabrication (easy shaping, patterning and integration).[10-13] As an important class of solid-state electrolytes, Ag-based ionic conductors have undergone several breakthroughs in recent years in enhancing the room temperature ionic conductivity.[14-17] In addition, the prototypes of all-solid-state batteries based on the silver fast ionic conductor were also reported.[18-21] However, to fulfill the requirements of commercial applications, the performances of such devices still need to be improved.

As a distinguished solid state electrolyte, the high-temperature α-phase AgI exhibits the super-ionic conductivity higher than 1 S·cm^{-1}, which is comparable with the liquid ones. However, upon cooling to 147 °C, the *α*-phase AgI will experience a structural transformation into the inferiorly conductive *β*- and *γ*-phase AgI, therefore restricting its uses. Various attempts have been performed to preventing the high-temperature α-phase AgI from transforming into the low-phase.

For example, using a traditional melt-quenching method, at room temperature, the high-temperature *α*-phase AgI can be kept in an $AgI\text{-}Ag_2O\text{-}B_2O_3$ glass matrix.[22] However, the high-temperature *α*-phase AgI will vanish upon a heating cycle.

Through a chemo-mechanical milling process, an enhancement of three orders of magnitude in ionic conductivity for the amorphous Ag_3PS_4 sample compared to the corresponding crystal phase was recently achieved by our group.[13] In this work, through the addition of AgI to Ag_3PS_4, we prepared the amorphous $0.5AgI\cdot0.5Ag_3PS_4$ sample via the high-energy ball-milling method, and this sample exhibited the ionic conductivity of 1.1×10^{-3} S·cm^{-1}. By subjecting the amorphous $0.5AgI\cdot0.5Ag_3PS_4$ to a certain degree of heat-treatment, a nano-crystal containing composite was obtained, which displayed an room temperature ionic conductivity of 3.9×10^{-3} S·cm^{-1}, i.e., approximately 4 times higher than that of the not heat-treated sample. By conducting structural characterizations, we observed and analyzed the atomic-scale structural evolutions from the crystalline to the amorphous $0.5AgI\cdot0.5Ag_3PS_4$ phase and further to the nano-crystalline composite. This enabled us to reveal the structural origins of the enhancement in ionic conductivity induced by both amorphization and heat-treatment.

Results

To determine its thermodynamic characteristics, calorimetric curves of the as-prepared $0.5AgI\cdot0.5Ag_3PS_4$ powder are shown in Fig.1. In the first up-scan curve, besides three clear exothermic peaks located at 137 °C, 197 °C, and 370 °C respectively, we can also see four smaller exothermic responses at 103, 260, 302 and 333 °C respectively.

According to the calorimetric responses of the as-prepared specimen, we selected the highest exothermal peak temperature of 370 °C as the annealing temperature. Utilizing an impedance analyzer, the comparison of complex impedance curves for both the as-synthesized sample and the isothermally heat-treated one are made in Fig.2. All curves display one semicircle in the high frequency region and a straight line in the low frequency region. The semicircle reflects the ionic conductivity *σ* (S·cm^{-1}) of the bulky materials, while the straight line is related to the characteristics of interface between the specimen and eletrode.

[a] *W. C. Qiao, Prof. H. Z. Tao, Prof. S. X. Gu, Dr. A. Qiao.*
State Key Laboratory of Silicate Materials for Architectures, Wuhan University of Technology, Wuhan 430070, China
E-mail: thz@whut.edu.cn
[b] *Y. H. Tao*
Wuhan Britain-China School, Wuhan 430034, China
[c] *Prof. Y. Z. Yue*
Department of Chemistry and Bioscience, Aalborg University, DK-9000 Aalborg, Denmark.
E-mail: yy@bio.aau.dk

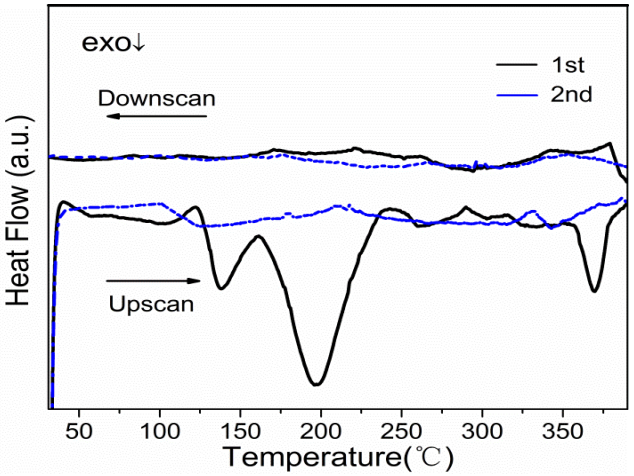

Fig. 1. Two runs of DSC up- and downscan curves for the 0.5AgI·0.5Ag$_3$PS$_4$ powder prepared via milling at 800 rpm for 10 hrs. Up-and downscan rates are 10 °C min^{-1}.

The electrical resistances of the sample at various temperatures can be respectively found by reading the difference of the two intercepts of the semicircle on *Z*' axis, i.e., by reading the diameter of the semicircle. σ can be obtained from the equation:

$$\sigma = \frac{L}{RS} \quad (1)$$

where *L* (cm) is the thickness of the plate, *R* (Ω) is the sample resistance, and *S* (cm^2) stands for the area of the electrodes. From Fig. 2 and equation (1), the room temperature ionic conductivity of the as-synthesized 0.5AgI·0.5Ag$_3$PS$_4$ powder was enhanced by about 4 times through the isothermal treatment at 370 °C for 20 min, i.e., from 1.1×10^{-3} to 3.9×10^{-3} S·cm^{-1}. This enhancement is associated with the drop of the activation energy (E_a) from 0.295 eV to 0.244 eV as a result of isothermal heat-treatment. As shown in Fig.2, E_a can be calculated by fitting the obtained σ (Fig.3) to the Arrehnian equation,[23,24]:

$$\sigma T = Aexp(-\frac{E_a}{kT}) \quad (2)$$

where σ is the total conductivity of the solid conductor at the temperature *T*, *k* is the Boltzmann constant, and *A* is the pre-exponential factor.

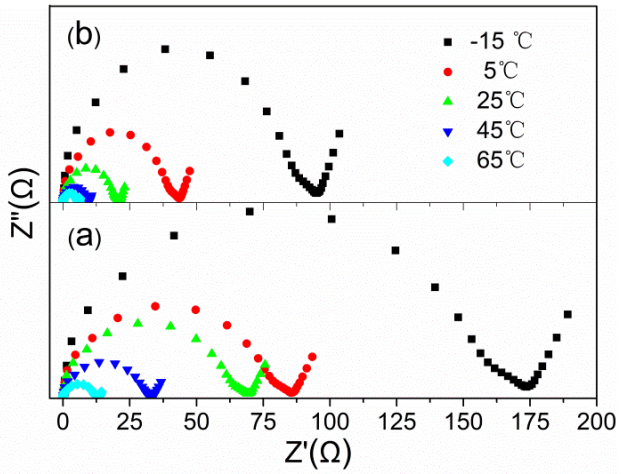

Fig. 2. Temperature dependence of the complex impedance for (a) the as-synthesized amrophous 0.5AgI·0.5Ag$_3$PS$_4$ powder and (b) the heat-treated one. The heat-treatment procedure is as follows: the as-synthesized powder was heated up to 370 °C at 5 °C min^{-1}, then held at 370 °C for 20 min, finally cooled down to room temperature by turning off the furnace.

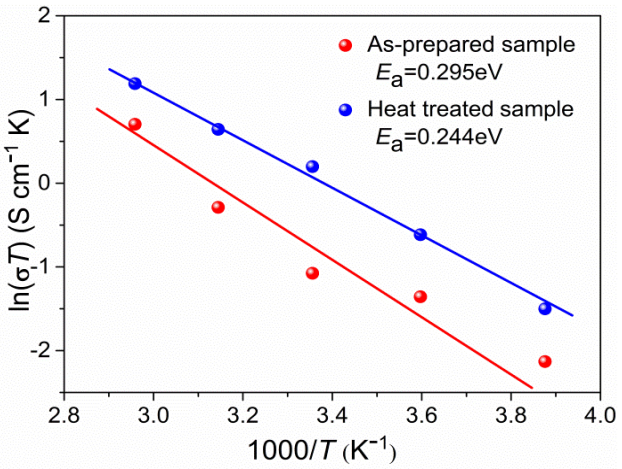

Fig. 3. Arrhenius plots of the ionic conductivity for both the as-synthesized amorphous 0.5AgI·0.5Ag$_3$PS$_4$ powder and the sample heat-treated at 370 °C for 20 min.

To investigate the atomic-scale origin of these calorimetric responses upon heating and the mechanism of the enhancement of the ionic conductivity, several structural characterization techniques were utilized. XRD patterns were obtained for both the as-prepared 0.5AgI·0.5Ag$_3$PS$_4$ powder and those treated at 150 °C, 250 °C and 370 °C, respectively, for 20 min. In addition, Raman and ^{31}P solid NMR spectra of the as-prepared 0.5AgI·0.5Ag$_3$PS$_4$ powder and the heat-treated one at 370 °C for 20 min were shown in Figs. 5 and 6 to probe the structural difference of the two samples. Finally, to identify the structural difference between the as-prepared 0.5AgI·0.5Ag$_3$PS$_4$ powder and the previously reported amorphous Ag$_3$PS$_4$ powder[13], Ag K-edge XANES and EXAFS spectra were also obtained as seen in Fig.7.

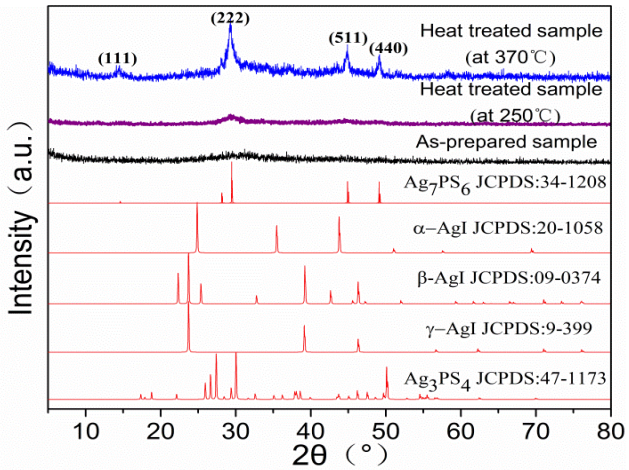

Fig. 4. XRD patterns of the as-synthesized 0.5AgI·0.5Ag_3PS_4 powder and the heat-treated ones. The heat-treated protocol is as follows: the as-synthesized powder was heated at 5 °C min^{-1} to a temperature (250 °C or 370 °C), then holding at this temperature for 20 min, finally cooling to room temperature through turning off the power.

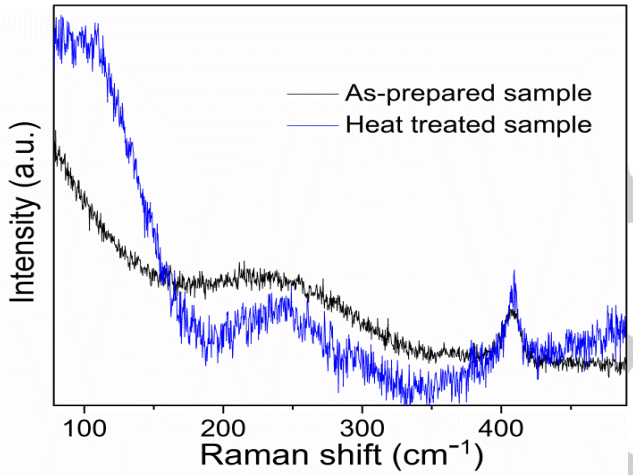

Fig.5. Raman spectra of the as-synthesized 0.5AgI·0.5Ag_3PS_4 powder (black) together with the one heat-treated at 370 °C for 20 min (blue).

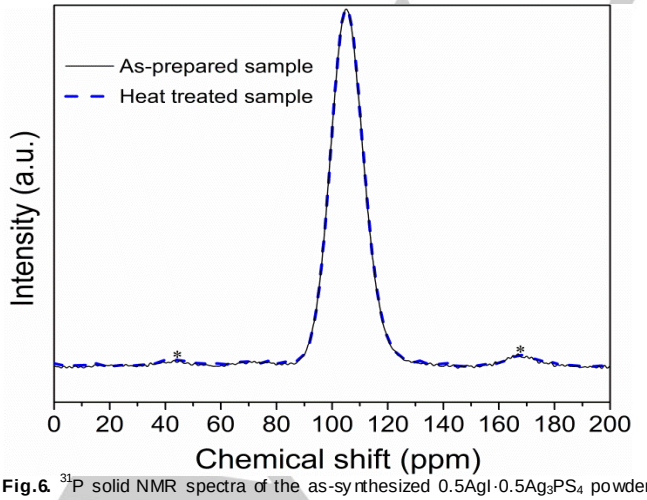

Fig.6. ^{31}P solid NMR spectra of the as-synthesized 0.5AgI·0.5Ag_3PS_4 powder together with (b) the one heat-treated at 370 °C for 20 min. Spinning sidebands are designated by asterisks.

Discussion

Calorimetric responses

In this work, we observed several fascinating phenomena in the DSC curves of the as-prepared 0.5AgI·0.5Ag_3PS_4 sample (Fig. 1), in strong contrast to the amorphous Ag_3PS_4 reported in our previous work.[25]

First, as confirmed by the XRD patterns of the heat-treated ones, the 0.5AgI·0.5Ag_3PS_4 sample still remains amorphous after heat-treatment at 250 °C for 20 min. Therefore, two distint exothermic peaks occur at 137 °C and 197 °C respectively during the first upscan (Fig. 1), which could be due to the two stages of relaxation of the distorted amorphous 0.5AgI·0.5Ag_3PS_4. According to the structural characterizations, the ionic bonding occurs in the 0.5AgI·0.5Ag_3PS_4 sample owing to the presence of Ag^+, I^-, and $[PS_4]^{3-}$ ions. The exothermic peaks at 137 °C could be attributed to the relaxation of the distorted Ag{$[PS_4]_mI_n$} polyhedral units, whereas the peak at 197 °C could be assigned to the relaxation of the distorted [PS_4] tetrahedral units. These assignments were also reported for the as-prepared amorphous Ag_3PS_4.[25]

econd, according to the XRD pattern of the sample heat-treated at 370 °C for 20 min (Fig. 4), the exothermic peak at 370 °C (Fig. 1) should be assigned to the formation of the single Ag_7PS_6 crystal, in contrast to the precipitated crystalline Ag_3PS_4 phase in the milling-induced amorphous Ag_3PS_4 powder. In addition, the crystallization peak for the as-prepared amorphous 0.5AgI·0.5Ag_3PS_4 powder is much smaller than the relaxation peaks (Fig. 1), and this scenario is different from that of the amorphous Ag_3PS_4, where the crystallization peak is stronger than the relaxation peak. This difference could be due to the enhanced structural disorder and heterogeneity upon adding AgI.

Finally, similar to the case for the Ag_3PS_4 amorphous sample,[25] a glass transition cannot be detected prior to the crystallization peak for the amorphous 0.5AgI·0.5Ag_3PS_4 powder.

Atomic-scale structural origin of the enhancement in ionic conductivity

Compared to the as-prepared amorphous Ag_3PS_4 powder,[13] the addition of AgI to Ag_3PS_4 following the stoichiometric ratio of 0.5AgI·0.5Ag_3PS_4 leads to a large jump of the room temperature (298 K) ionic conductivity, i.e., an increase from 8.5×10^{-4} S·cm^{-1} to 1.1×10^{-3} S·cm^{-1} (Fig. 2). This enhancement could be mainly ascribed to the drop in the activation energy (E_a) from 0.320 eV for the as-prepared Ag_3PS_4 amorphous powder to 0.295 eV for the 0.5AgI·0.5Ag_3PS_4 amorphous powder.

Now the central question arises: what is the atomistic origin of the enhancement in ionic conductivity by adding AgI? To answer this question, the comparison in the Ag K-edge XANES and EXAFS spectra between the as-prepared amorphous Ag_3PS_4 and 0.5AgI·0.5Ag_3PS_4 powders are made in Fig. 7. It turns out that only a small difference between the two samples

can be seen in the Ag K-edge XANES spectra, implying the changes in the coordinating surroundings around Ag^+ ions. Furter information about the nearest neighbor coordinating species can be deduced from the peak located at 2.7 Å near the Ag-S peak in the Ag K-edge EXAFS spectra (Fig. 7b), implying a formation of Ag-I bonds upon adding AgI. This suggests that the nearest neighbor surroundings of Ag^+ ions from $[PS_4]$ single anions transform into the $\{[PS_4]_m I_n\}$ mixed polymeric anions. Based on the model presented elsewhere,[26,27] the enhancement in ionic conduction (originating from mixed iodine and oxygen environments) upon adding AgI to an oxide glass system could be ascribed to the increase in the I-Ag distance, since oxygens draw Ag^+ ions, and thereby increase the average I-Ag distance. In this work, the rise in ionic conductivity could be also ascribed to the extension of the pathways for ionic transport due to the formation of $\{[PS_4]_m I_n\}$ mixed polymeric anions. The asymmetry of the nearest neighbor surroundings of Ag^+ ions facilitates the migration of Ag^+ ions.

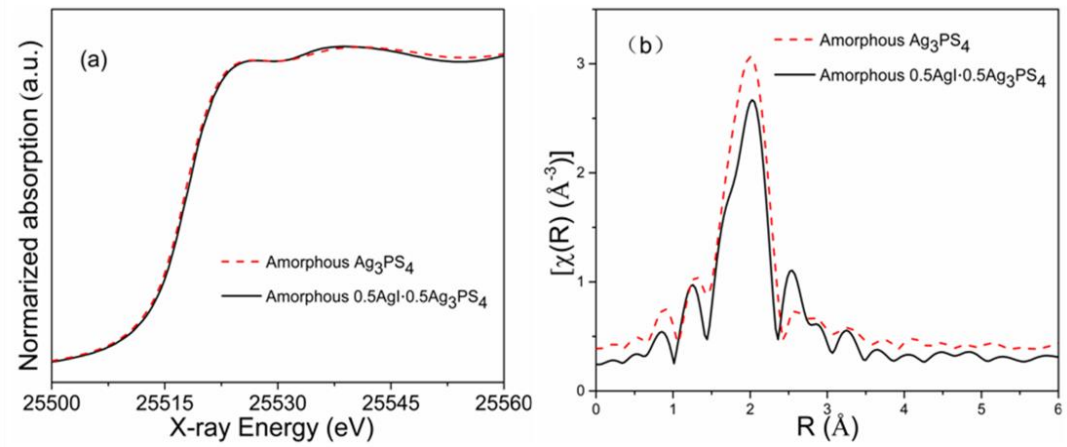

Fig.7. XANES (a) and EXAFS spectra in R-space (b) for Ag K-edge of the as-synthesized amorphous Ag_3PS_4 and 0.5AgI·0.5Ag_3PS_4 powders.

The further enhancement (about 4 times) in room temperature ionic conductivity upon heat-treatment at 370 °C for 20 min for the amorphous 0.5AgI·0.5Ag_3PS_4 powder could be attributed to the following aspects. First, different from the precipitated Ag_3PS_4 crystal phase in the as-synthesized Ag_3PS_4 amorphous powder, Ag_7PS_6 crystal phase (JCPDS 41-0866) appears in the heat-treated amorphous 0.5AgI·0.5Ag_3PS_4 powder as confirmed by the XRD pattern shown in Fig. 4. It has been reported that the ionic conductivity of Ag_7PS_6 crystal is 1.5×10^{-6} S·cm^{-1},[28] which is much lower than those of both the amorphous 0.5AgI·0.5Ag_3PS_4 powder (1.1×10^{-3} S·cm^{-1}) and the heat-treated amorphous 0.5AgI·0.5Ag_3PS_4 powder (3.9×10^{-3} S·cm^{-1}). According to the stoichiometry of the 0.5AgI·0.5Ag_3PS_4 amorphous powder, given the complete precipitation of the Ag_7PS_6 crystal phase, the composition of the residual amorphous phase should be $AgPS_2I_2$, and the latter exhibits a room temperature ionic conductivity of about $1.1\sim3.3\times10^{-3}$ S·cm^{-1}.[29,30] This value is also lower than that of the heat-treated amorphous 0.5AgI·0.5Ag_3PS_4 powder (3.9×10^{-3} S·cm^{-1}). Thus, another question arises: What else causes the further enhancement of the room temperature ionic conductivity for the heat-treated amorphous 0.5AgI·0.5Ag_3PS_4 powder?

Based on the investigations on the Li^+ solid-state electrolyte,[31-33] the enhancement in ionic conductivity might be realized through the formation of a certain crystal phase with a lower ionic conductivity in the amorphous sample. This anomalous behavior could be clarified by considering the role of interface between the crystalline and the amorphous phases in influencing the ionic conductivity of the composite, e.g.,through the formation of percolative conductive pathways, the aggregation of transferring ions, and space charges. According to a previous study,[34] two possibilities might explain the anomalous phenomenon. On one hand, the severe lattice deformations could lead to the enhanced ionic transportation in the interfacial region. On the other hand, the rise of transferring ions in quantity in the interfacial regions could also contribute to the enhancement in ionic conductivity. Therefore, when the size of the crystallites is reduced to nano-scale, the interconnected interfacial regions benefit the formation of percolative pathways for ionic transportation in the composite. Such a strong enhancement in ionic conductivity caused by interfacial effects has been observed in many nano-crystals containing composites.[35,36]

In addition, due to the higher binding energy of P-S bonds, the polymerized anions $[PS_4]$ tetrahedra are preserved in the as-prepared amorphous 0.5AgI·0.5Ag_3PS_4 powder and the heat-treated one, deduced from the similar characteristic Raman peaks for $[PS_4]$ tetrahedral[13,37-39] (Fig. 5) and the similar ^{31}P NMR spectra (Fig. 6).

According to the above-mentioned explanations, the mechanisms of the enhancement in ionic conductivity are schematically illustrated in Fig. 8.

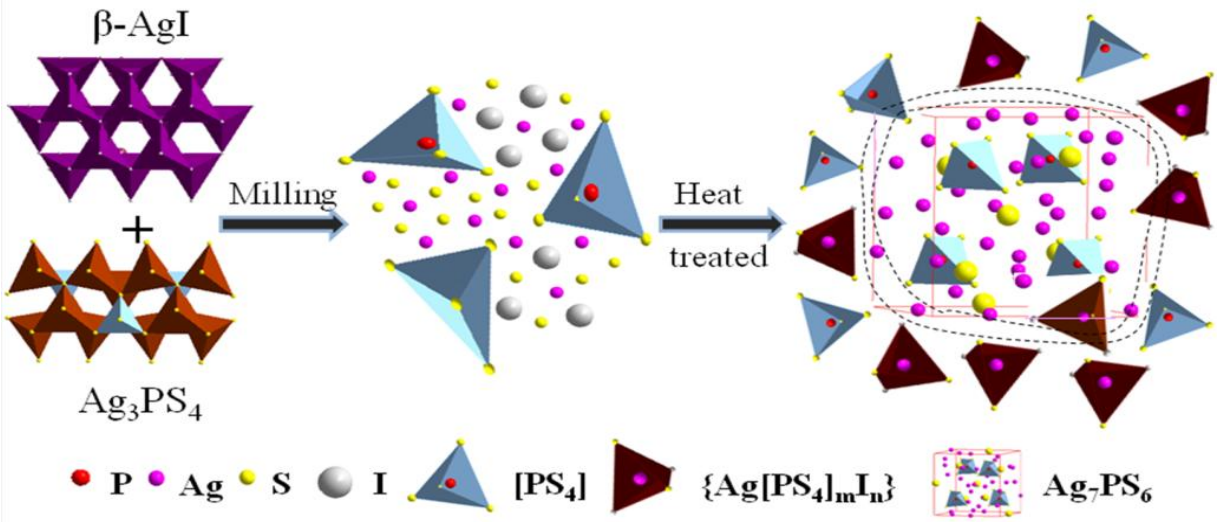

Fig.8. Schematic diagrams of the structural evolution from the initial crystals, to amorphous materials upon milling, and finally to nano-crystal composites obtained by heat-treatment at 370 °C for 20 min.

Conclusions

We synthesized a new kind of the Ag-based fast ionic conductor, i.e., the amorphous $0.5AgI{\cdot}0.5Ag_3PS_4$, via a chemo-mechanical ball milling. Compared to the Ag_3PS_4 amorphous powder, the addition of equal molar AgI to Ag_3PS_4 strongly enhances the room temperature ionic conductivity, i.e., up to 1.1×10^{-3} $S{\cdot}cm^{-1}$ for the amorphous $0.5AgI{\cdot}0.5Ag_3PS_4$ powder. Further enhancement of about 4 times was realized upon the heat-treatment of the amorphous $0.5AgI{\cdot}0.5Ag_3PS_4$ powder at 370 °C for 20 min. The detailed structural characterizations allowed us to reveal the atomistic origin of the ionic conductivity enhancement upon adding AgI to the amorphous Ag_3PS_4, i.e., the formation of $\{[PS_4]_m I_n\}$ mixed polymeric anions around Ag^+ ions in the amorphous $0.5AgI{\cdot}0.5Ag_3PS_4$ powder plays a crucial role. We found the precipitation of Ag_7PS_6 crystal phase in the heat-treated amorphous $0.5AgI{\cdot}0.5Ag_3PS_4$ powder. Finally, based on the detailed structural analysis, we established the mechanisms of the enhancement in ionic conductivity for both the amorphous $0.5AgI{\cdot}0.5Ag_3PS_4$ powder and the heat-treated one. This work will be useful for the design and production of the silver-based super-ionic electrolytes.

Experimental Section

Sample preparation

The amorphous Ag_3PS_4 and $0.5AgI{\cdot}0.5Ag_3PS_4$ samples were prepared through a chemo-mechanical milling equipment (Pulverisette-7 premium line; Fritsch, Idar-Oberstein, Germany) at 800 rpm for 10 hours. Reagent-grade AgI, Ag_2S and P_2S_5 (all from Aladdin, Shanghai, China) crystalline powders were used as starting materials. Then these powders were loaded into a 20ml ZrO_2 pot with Φ 3 mm ZrO_2 balls according to the ~1:15 weight ratio between the sample and balls. The detailed procedure was reported elsewhere.[13, 40, 41]

Characterizations

To detect the calorimetric responses of the as-prepared $0.5AgI{\cdot}0.5Ag_3PS_4$ powder and the appropriate heat-treated parameters, two rund of DSC up- and downscan at 10 °C min^{-1} were conducted by utilizing a differential scanning calorimeter (DSC) (Netzsch STA449 F1, Netzsch, Selb, Germany).

The amorphous nature of the as-synthesized $0.5AgI{\cdot}0.5Ag_3PS_4$ samples, as well as the precipitated crystal phases in the heat-treated samples, were determined by an X-ray diffractometer (Rigaku, RU-200B, Tokyo, Japan) with Cu K_α radiation at a voltage of 40 kV and a current of 40 mA, and the X-ray diffraction (XRD) patterns were recorded in the 2θ range of 5-80°. In addition, structure investigation was conducted using a HORIBA LabRAM HR Evolution Raman microscope, in which a 633 nm laser with a typical power lower than 5 mW was used to avoid the laser-induced damage. Furthermore, the nearest neighboring environments of Ag in both the as-synthesized Ag_3PS_4 and the $0.5AgI{\cdot}0.5Ag_3PS_4$ sample were characterized by the Ag K-edge X-ray absorption near edge structure (XANES) and the extended X-ray absorption fine structure (EXAFS) spectra. The details about the measurement can be found elsewhere.[13,42] Finally, the local coordination surroundings of P for both the as-synthesized and the heat-treated $0.5AgI{\cdot}0.5Ag_3PS_4$ samples were probed by the ^{31}P MAS NMR experiments. These measurements were conducted at 120 MHz on a Bruker Avance III 400 spectrometer furnished with a 4 mm probe. The ^{31}P chemical shifts are referenced to 85% H_3PO_4 aqueous solution (δ = 0 ppm).

To characterize the electrochemical performances, the as-synthesized powders were dry-pressed vertically into plates with a diameter of 1.28 cm and with a height of about 0.1 cm. Through magnetron sputtering technique, the two sides of the

obtained plates were coated with a layer of platinum films. The AC impedance spectra of both the as-synthesized and the heat-treated samples were obtained using an impedance analyzer (Solartron, 1260A) in the frequency range from 0.1 Hz to 10 MHz using an amplitude voltage of 50 mV across the sample. These measurements were carried out in the temperature range of -15 °C to 65 °C under an atmospheric condition. The ionic conductive performance was analyzed by using the Z-View impedance software.

Acknowledgements

This work was financially supported by NSFC (Nos.51772223, 51372180). We are grateful to Xiujian Zhao and Xianghua Zhang (Wuhan University of Technology) for valuable discussions. W.C. Qiao and A. Qiao contributed equally to this work. In addition, we also acknowledge the provision of synchrotron access to Beamline BL14W1 at the Shanghai Synchrotron Radiation Facility.

Keywords: Solid electrolyte; Ionic conductivity; EXAFS; High-energy ball-milling

[1]. M. Armand, J. M. Tarascon, *Nature.* **2008**, *451*, 652–657.
[2]. J. M. Tarascon, M. Armand, *Nature*. **2001**, *414*, 359–367.
[3]. W. Hou, X. Guo, X. Shen, K. Amine, H. Yu, J. Lu, *Nano Energy*. **2018**, *52*, 279–291.
[4]. K. H. Park, D. Y. Oh, Y. E. Choi, Y. J. Nam, L. Han, J. Kim, H. Xin, F. Lin, S. M. Oh, Y. S. Jung, *Adv. Mater*. **2016**, *28*, 1874–1883.
[5]. J. Janek, W. G. Zeier, *Nat. Energy*. **2016**, *1*, 1–4.
[6]. J. B. Goodenough, K. Park, *J. Am. Chem. Soc*. **2013**, *135*, 1167–1176.
[7]. F. Strauss, T. Bartsch, L. Biasi, A. Y. Kim, J. Janek, P. Hartmann, T. Brezesinski, *ACS Energy Lett*. **2018**, *3*, 992–996.
[8]. T. Asano, A. Sakai, S. Ouchi, M. Sakaida, A. Miyazaki, S. Hasegawa, *Adv. Mater*. **2018**, *1803075*, 1–7.
[9]. K. Takada, *Acta Mater*. **2013**, *61*, 759–770.
[10]. M. Park, X. Zhang, M. Chung, G. B. Less, A. Marie, *J. Power Sources*. **2010**, *195*, 7904–7929.
[11]. M. Wakihara, *Mater. Sci. Eng.*. **2001**, *R33*, 109–134.
[12]. K. Zaghib, P. Charest, A. Guerfi, J. Shim, M. Perrier, K. Striebel, *J. Power Sources*. **2004**, *134*, 124–129.
[13]. A. Qiao, H. Tao, Y. Yue, *J. Non-Cryst. Solids*. **2019**, *521*, 119476.
[14]. K. Terabe, T. Hasegawa, T. Nakayama, M. Aono, *Nature*. **2005**, *433*, 47–50.
[15]. H. Zhang, T. Tsuchiya, C. Liang, K. Terabe, *Nano Lett*. **2015**, *15*, 5161–5167.
[16]. C. Lin, E. Zhu, J. Wang, X. Zhao, F. Chen, S. Dai, *J. Phys. Chem. C*. **2018**, *122*, 1486–1491.
[17]. R. Makiura, T. Yonemura, T. Yamada, M. Yamauchi, R. Ikeda, H. Kitagawa, K. Kato, M. Takata, *Nat. Mater*. **2009**, *8*, 476–480.
[18]. P. Boolchand, W. J. Bresser, *Nature*. **2001**, *410*, 1070–1073.
[19]. R. Murugaraj, G. Govindaraj, S. Ramasamy, *J. Power Sources*. **2002**, *112*, 184–190.
[20]. B. K. Heep, K. S. Weldert, Y. Krysiak, T. W. Day, W. G. Zeier, U. Kolb, G. J. Snyder, W. Tremel, *Chem. Mater*. **2017**, *29*, 4833–4839.
[21]. C. Lin, C. Rüssel, S. Dai, *Prog. Mater. Sci*. **2018**, *93*, 1-44.
[22]. M. Tatsumisago, Y. Shinkuma, T. Minami, *Nature*. **1991**, *354*, 217–218.
[23]. Z. Zhang, J. H. Kennedy, *J. Electrochem. Soc*. **1993**, *140*, 2384–2390.
[24]. W. Yao, S.W. Martin, *Solid State Ionics*. **2008**, *178*, 1777–1784.
[25]. A. Qiao, H. Tao, Y. Yue, *J. Am. Ceram. Soc*. **2017**, *100*, 968–974.
[26]. P. Mustarelli, C. Tomasi, A. Magistris, *J. Phys. Chem. B*. **2005**, *109*, 17417–17421.
[27]. S. Adams, J. Swenson, *Phys. Rev. B*. **2000**, *63*, 1–11.
[28]. Z. M. Zhang, J. H. Kenned, *J. Electrochem. Soc*. **1993**, *140*, 2384-2390.
[29]. H. Tao, S. Yan, P. Wang, A. Qiao, C.N. Patent **2016**, 106057276A.
[30]. H. Tao, P. Wang, A. Qiao, C. Zhong, Y. Yue, C.N. Patent 2015, 104752756A.
[31]. F. Su, *Solid State Ionics*. **1982**, *7*, 37-41.
[32]. L. Q. Chen, L. Z. Wang, G. C. Che, G. Wang, Z. R. Li, *Solid State Ionics*. **1984**, *14*, 149-152.
[33]. U. M. Gundusharma, E. A. Secco, *Solid State Ionics*. **1990**, *44*, 47–50.
[34]. S. Adams, K. Hariharan, J. Maier, *Solid State Ionics*. **1995**, *75*, 193-201.
[35]. P. Knauth, J. M. Debierre, G. Albinet, *Solid State Ionics*. **1999**, *121*, 101–106.
[36]. G. Albinet, J. M. Debierre, P. Knauth, C. Lambert, L. Raymond, *Eur. Phys. J. B*. **2001**, *22*, 421–427.
[37]. I. P. Studenyak, V. O. Stefanovich, M. KranjEecb, D. I. Desnica, Y. M. Azhnyukd, G. S. Kovacsa, V. V. Panko, *Solid State Ionics*. **2003**, *95*, 221–225..
[38]. S. Jörgens, A. Mewis, *Solid State Sci*. **2007**, *9*, 213–217.
[39]. H. Andrae, R. Blachnik, *J. Alloy. Comp*. **1992**,*189*, 209–215.
[40]. Y. Katayama, S. Hama, T. Yanagihara, M. Hayashi, U.S. Patent **2011**, 20110049745A1.
[41]. S. Hama, M. Hayashi, U.S. Patent **2013**, 8, 556, 179.
[42]. M. Newville, *J. Synchrotron Radiat*. **1998**, *8*, 322–324.

ARTICLE

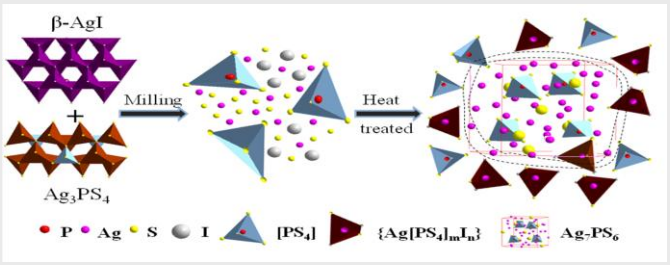

*W. C. Qiao, H. Z. Tao**

Page No. – Page No.

Structural origins of the enhancement in ionic conductivity of a chalcogenide compound by adding AgI

The back cover picture reveals the mechanisms of the enhancement in ionic conductivity for the present $0.5AgI{\cdot}0.5Ag_3PS_4$ amorphous powder together with the heat-treated one are schematically given.